LRP 354/88 September 1988

TDA - A three-dimensional axisymmetric code for free-electron-laser (FEL) simulation

T.M. Tran and J.S. Wurtele

TDA – A three-dimensional axisymmetric code for free-electron-laser (FEL) simulation

T.M. Tran

Centre de Recherches en Physique des Plasmas

Association Euratom-Confédération Suisse

Ecole Polytechnique Fédérale de Lausanne

21, Av. des Bains, CH-1007 Lausanne

and

J.S. Wurtele

Department of Physics and Plasma Fusion Center

Massachusets Institute of Technology

Cambridge, MA 02139

A particle simulation code, TDA, which models the single-pass amplification process in a free-electron-laser (FEL) is developed and tested. The code allows for the treatment of the fully three-dimensional electron dynamics, thus taking into account the transverse betatron motion as well as the longitudinal bunching of the electrons. The paraxial wave equation that governs the growth and the diffraction of the self-consistent radiation field (assumed to be axisymmetric), is discretized in the radial direction by the finite difference method. The benchmark study indicates that the single-pass gain, as well as the optical guiding phenomena can be well described by the code with a reasonable number of simulation particles ($N \sim 1000$) and a radial mesh number not exceeding 64. A detailed discussion of the numerical method is presented.

1. Introduction

The single particle description of the free-electron-laser (FEL), in which the single particle orbits and the eikonal electromagnetic field amplitude interact self-consistently, has been utilized successfully to investigate FEL performance in the Compton regime [1–6], and the collective (Raman) regime [7, 8]. One of its advantages is its inherent simplicity that allows the inclusion of many complex physical effects encountered in real experimental conditions such as wave diffraction, non-uniform wiggler, non-ideal electron beams and nonlinear electron motion.

In this paper, we are concerned with the simulation of the single-pass gain process in the FEL in which the self-consistent transverse behavior of the radiation field (diffraction, optical guiding) as well as the fully three-dimensional dynamics of the electrons (emittance, transverse betatron motion due to the non-uniform wiggler transverse profile) are investigated. The code, named TDA, which results, can be viewed as a first step to the development of more complex codes that can handle others effects such as the multiple passes in an FEL oscillator, electrostatic perturbations, non-axisymmetric radiation field when the electron beam is not perfectly circular. Similar FEL codes exist [8, 9] and they have been used to study short wavelength FELs. The purpose of this paper is to discuss in detail the numerical techniques involved in implementing such a model.

A brief description of the physical model studied with the TDA code is outlined in Sec.2, followed in Sec.3 by the details of the numerical methods employed for the particle initialization, the discretization of the paraxial wave equation in the radial direction and the numerical integration along the direction of the beam propagation z. In Sec.4, we benchmark the code (a) by comparing the simulation results with the predictions of the linear theory and (b) by performing a convergence study for the radial discretization. Finally, the conclusions are presented in Sec.5.

2. Physical model

In the free-electron-laser, the single-pass gain mechanism can be well described by the relativistic single-particle equations of motion, coupled to the paraxial wave equation for the radiation field. It is also assumed that only one radiation frequency is present in the system, so that the fast wiggle oscillations of the electrons are averaged out. Futhermore, we consider an electron beam which is sufficiently tenuous that the longitudinal electrostatic perturbations are negligible (Compton regime assumptions).

2.1 Equations of motion

The longitudinal motion (averaged over the wiggle period) is governed by the following equations for the Lorentz factor γ and the electron phase $\theta = (k_s + k_w)z - (\omega_s - \omega_w)t$ [2, 3, 8, 10]:

$$\frac{d\gamma}{dz} = -k_s \left(1 - \frac{\omega_w}{ck_s}\right) \frac{a_w a_s f_B \sin(\theta + \phi_s)}{\gamma}, \tag{1.a}$$

$$\frac{d\theta}{dz} = k_w + \frac{\omega_w}{c} - k_s \left(1 - \frac{\omega_w}{ck_s}\right) \frac{1 + a_w^2 + p_x^2 + p_y^2 + 2a_w a_s f_B \cos(\theta + \phi_s)}{2\gamma^2}. \tag{1.b}$$

In these equations, the radiation (or signal) field is characterized by the wavenumber $k_s = 2\pi/\lambda_s = \omega_s/c$, the dimensionless vector potential rms value $a_s = eA_s/mc$ and the phase ϕ_s, while the wiggler field is specified by the frequency ω_w, axial wavelength k_w and vector potential $a_w = eB_w/mck_w$. Assuming that $\omega_w \neq ck_w$ allows for the treatment of an electromagnetic wiggler in the free space configuration as well as in a waveguide. The usual equations for a magnetostatic wiggler field is recovered by setting $\omega_w = 0$ in Eqs.(1). For a helical wiggler, the coefficient $f_B = 1$ and in the planar wiggler f_B is a sum of Bessel functions given by:

$$f_B = J_0\left[\frac{a_w^2}{2(1 + a_w^2)}\right] - J_1\left[\frac{a_w^2}{2(1 + a_w^2)}\right].$$

In Eq.(1.b), p_x, p_y are the averaged transverse canonical momenta normalized to mc. For a given transverse profile of the wiggler field $a_w(x, y)$ and neglecting the effects of the radiation field, the momenta p_x, p_y evolve according to:

$$\frac{dp_x}{dz} = -\frac{1}{2\gamma}\frac{\partial}{\partial x}a_w^2, \tag{2.a}$$

$$\frac{dp_y}{dz} = -\frac{1}{2\gamma}\frac{\partial}{\partial y}a_w^2. \tag{2.b}$$

Finally the equations for the averaged transverse electron positions can be written as:

$$\frac{dx}{dz} = \frac{p_x}{\gamma}, \tag{3.a}$$

$$\frac{dy}{dz} = \frac{p_y}{\gamma}. \tag{3.b}$$

From Eqs.(2,3), it can be shown that the transverse electron motion (or betatron motion) has a constant of motion given by:

$$a_w^2(x,y) + p_x^2 + p_y^2 = \text{const.}$$

which shows explicitly that the magnetostatic wiggler (in which the transverse gradient of the field is positive) has a focusing effect on the electron propagation, while the electromagnetic wiggler (negative transverse gradient) can defocus the electron beam.

2.2 Wave equation

Assuming a single frequency and the paraxial approximation, the evolution of the slowly varying radiation field amplitude is governed by the following complex partial differential equation:

$$\left[\frac{\partial}{\partial z} + \frac{1}{2ik_s}\nabla_\perp^2\right] a_s e^{i\phi_s} = i\frac{eZ_0}{mc^2}\frac{f_B}{2k_s}\frac{I}{N}\sum_{j=1}^{N}\delta(x-x_j)\delta(y-y_j)a_w(x_j,y_j)\frac{e^{-i\theta_j}}{\gamma_j}, \tag{4}$$

where $Z_0 = 377\,\Omega$ is the vacuum impedance. In the right hand side of Eq.(4), we have assumed that each of the N simulation particles carries the partial current I/N. From Eqs.(1.a, 4), it is straightforward to derive the power balance equation:

$$P_b(z) + (1-\omega_w/ck_s)P_{\text{rad}}(z) = \text{const.}, \tag{5}$$

where the electron beam power P_b and the radiation power P_{rad} are defined by:

$$P_b = \frac{mc^2}{e}\frac{I}{N}\sum_{j=1}^{N}(\gamma_j - 1), \tag{6.a}$$

$$P_{\text{rad}} = \left(\frac{mc^2}{e}\right)^2 \frac{1}{Z_0}\iint k_s^2 a_s^2\, dxdy. \tag{6.b}$$

Note that the term proportional to ω_w/ck_s in the power balance equation (5) is the pump depletion in an electromagnetic wiggler [10] and can be important in a low energy FEL. From the practical point of view, the power balance Eq.(5) provides a useful diagnostic for the numerical simulation based on the self-consistent set of equations (1)–(4).

2.3 Initial conditions

The initial conditions for the particles are defined by specifying the electron distribution function on the 6-dimensional phase space $F(\gamma, \psi, p_x, x, p_y, y)$ at the entrance of the wiggler at $z = 0$. The phase ψ used in the distribution function is related to the previously defined phase θ by $\psi_j = \theta_j + \phi_s(x_j, y_j)$ for each electron j at a given axial position z. In the calculations presented at the end of this paper, the distribution F is assumed to be written as:

$$F(\gamma, \psi, p_x, x, p_y, y) = F_\gamma(\gamma) F_\psi(\psi) F_t(p_x, x, p_y, y), \tag{7}$$

where (a) F_γ is a Gaussian distribution, (b) F_ψ is uniform within the interval $[-\pi, \pi]$ and (c) F_t is uniform in the 4-D ellipsoid with minor axis R_x, Δp_x, R_y and Δp_y. Note that the normalized emittance in the x-direction can be expressed as $\epsilon_{nx} = R_x \Delta p_x$ and similarly for the emittance in the y-direction. The next section will describe in detail the method used in the code TDA to implement this distribution function.

For the initial radiation field profile, we assume a Gaussian TEM_{00} mode at $z = 0$. Recall that the propagation in vacuum for this mode is governed by [11]:

$$\begin{aligned} a_s(r,z) e^{i\phi_s(r,z)} &= \sqrt{\frac{2}{\pi}} a_{s0} \frac{w_0}{w(z)} e^{-r^2/w^2(z)} e^{i\varphi(r,z)}, \\ w^2(z) &= w_0^2 \left[1 + (z - Z_w)^2 / Z_R^2\right], \\ \varphi(r,z) &= -\tan^{-1}\left[(z - Z_w)/Z_R\right] + \frac{k_s r^2}{2} \frac{z - Z_w}{(z - Z_w)^2 + Z_R^2}, \end{aligned} \tag{8}$$

where w_0 is the minimum spot size, $Z_R = k_s w_0^2/2$ is the Rayleigh length and Z_w is the position of the radiation waist (focus). From the definition of P_{rad}, Eq.(6.b) and Eq.(8), the input power can be written in terms of a_{s0} as

$$P_{\mathrm{rad}}(0) = \left(\frac{mc^2}{e}\right)^2 \frac{k_s^2 w_0^2}{Z_0} a_{s0}^2. \tag{9}$$

Thus, the radiation beam at $z = 0$ is completely specified by giving the radiation wavelength, $\lambda_s = 2\pi/k_s$, the input power, $P_{\rm rad}(0)$, the Rayleigh length, Z_R (or the minimum spot size, w_0) and the position of the beam waist, Z_w since the complex radiation vector potential can be expressed at $z = 0$, as

$$a_s(r,0)e^{i\phi_s(r,0)} = \sqrt{\frac{2}{\pi}}a_{s0}\frac{w_0}{w(0)}e^{-Cr^2}, \qquad \text{with} \qquad C = \frac{k_s/2}{Z_R - iZ_w}. \tag{10}$$

3. Numerical method

3.1 Particle initialization

In order to simulate the distribution functions defined in Eq.(7) with a finite number of particles ($N \sim$ 1000–4000), three methods of particle loading are implemented in the TDA code:

(a) Loading using the pseudo-random numbers;

(b) Loading using the Hammersley's sequence [12] defined by:

$$\{(j-1/2)/N, \Phi_1(j), \Phi_2(j), \Phi_3(j), \ldots, \Phi_r(j), \ldots\}, \qquad j = 1, \ldots, N, \tag{11}$$

where $\Phi_r(j)$ denotes the radical inversion function in base r, with r being a prime number:

$$\Phi_r(j) = a_0 r^{-1} + a_1 r^{-2} + \cdots, \qquad j = a_0 + a_1 r^1 + \cdots; \tag{12}$$

(c) Loading using a "quiet start" scheme proposed in Ref.[9], where only a small number (typically 4) of phases ψ distributed evenly in $[-\pi,\pi]$ are filled with identical particle distributions in (γ, p_x, x, p_y, y); these distributions are constructed by using either method (a) or method (b).

In agreement with [9], the last method is found to be most effective in the small signal $[P_{\rm rad}(0) \ll P_b(0)]$ high gain (exponential) regime. The methods (a) and (b) are more suitable in both the low gain regime ($G \approx 1$) and the near-saturation regime. In

practice, we prefer the method (b) because it produces less noise for a small number N of sampling particles.

A nonuniform particle distribution function $F(x)$ (a Gaussian function for example) is sampled by assigning its cumulative distribution to a set of uniform distribution of numbers R_j with $0 < R_j < 1$ (which are sampled by using the loading schemes described above)

$$\int_0^{x_j} F(x')\,dx' \Big/ \int_0^1 F(x')\,dx' = R_j. \tag{13}$$

The value of the variable x_j can then be computed by inverting Eq.(13) numerically (see for example [13]).

3.2 Discretization of the wave equation

In TDA, we assume that the radiation field is axisymmetric although the electron dynamics is fully 3-D. This assumption is exact in a helical wiggler; for a planar wiggler, it is still a good approximation if an appropriate focusing system is provided in order to maintain a nearly circular electron beam [14]. This additional focusing effect can be easily included in the right hand side of the momentum equations, Eqs.(2).

Let subdivide the r-axis into N_r intervals (not necessary equal) bounded by $r_{k+1/2}$, $k = 0, \ldots, N_r$ with $r_{1/2} = 0$ and $r_{N_r+1/2} = R_{\max}$. The value of $R_{\max}$ is chosen such that it is several times larger than the initial radiation beam size $w(0)$ and the initial electron beam radius. Then, define the "volume" $V_k \equiv \pi(r_{k+1/2}^2 - r_{k-1/2}^2)$, the "area" $A_{k+1/2} \equiv 2\pi\, r_{k+1/2}$ and the mid-point $r_k \equiv (r_{k-1/2} + r_{k+1/2})/2$. Integration of the wave equation (4) in the "volume" V_k yields:

$$V_k \frac{da_k}{dz} + \frac{1}{2ik_s}\left[A_{k+1/2}\left(\frac{\partial a}{\partial r}\right)_{r_{k+1/2}} - A_{k-1/2}\left(\frac{\partial a}{\partial r}\right)_{r_{k-1/2}}\right] = i\frac{eZ_0}{mc^2}\frac{f_B}{2k_s}\frac{I}{N}\sum_{j\in\mathcal{J}_k} a_w(x_j, y_j)\frac{e^{-i\theta_j}}{\gamma_j}, \tag{13}$$

where

$$a_k \equiv \frac{2\pi}{V_k}\int_{r_{k-1/2}}^{r_{k+1/2}} a_s e^{i\phi_s}\, r\,dr \simeq a_s(r_k, z)e^{i\phi_s(r_k,z)}. \tag{14}$$

In Eq.(13), $\mathcal{J}_k$ denotes the set of indices of particles that are located inside the interval $[r_{k-1/2}, r_{k+1/2}]$. At $k = N_r$, we set directly in Eq.(13) the natural boundary condition $r\partial a/\partial r = 0$, which is consistent with the choice of a large value of $R_{\max}$ while at $k = 1$, the term containing $A_{1/2}$ is equal to zero. Note that no approximation has been introduced so far in Eq.(13). To proceed, the partial derivatives in Eq.(13) are discretized by the central differences as follows:

$$\left(\frac{\partial a}{\partial r}\right)_{r_{k+1/2}} \longrightarrow \frac{a_{k+1} - a_k}{r_{k+1} - r_k}. \tag{15}$$

Substituting Eq.(15) into Eq.(13) and dividing by $V_{k+1/2}$ yield the following system of N_r ordinary differential equations:

$$\begin{aligned}\frac{da_k}{dz} = {} & \frac{i}{2k_s}\sum_{k'=1}^{N_r} M_{k,k'}\, a_{k'} \\ & + \frac{i}{V_k}\frac{eZ_0}{mc^2}\frac{f_B}{2k_s}\frac{I}{N}\sum_{j\in\mathcal{J}_k} a_w(x_j, y_j)\frac{e^{-i\theta_j}}{\gamma_j}, \qquad k = 1, \ldots, N_r,\end{aligned} \tag{16}$$

where the real tridiagonal finite difference matrix $M_{k,k'}$ has the following elements:

$$M_{k,k-1} = \frac{1}{V_k}\frac{A_{k-1/2}}{r_k - r_{k-1}}, \quad M_{k,k+1} = \frac{1}{V_k}\frac{A_{k+1/2}}{r_{k+1} - r_k}, \quad M_{k,k} = -M_{k,k-1} - M_{k,k+1}. \tag{17}$$

It is straightforward to show that the matrix $M_{k,k'}$ verifies the identity:

$$\sum_{k=1}^{N_r} V_k a_k^* \sum_{k'=1}^{N_r} iM_{k,k'}a_{k'} + \text{c.c.} = 0. \tag{18}$$

To the same order of accuracy as in Eq.(14) or Eq.(15), the integral appearing in the radiation power definition, Eq.(6.b), can be discretized by

$$\iint a_s^2\, dx\, dy \longrightarrow \sum_{k=1}^{N_r} V_k |a_k|^2. \tag{19}$$

Use of Eq.(18) leads then to:

$$\frac{d}{dz}P_{\text{rad}} = -\frac{mc^2}{e}\frac{I}{N}\sum_{k=1}^{N_r}\sum_{j\in\mathcal{J}_k} f_B a_w(x_j, y_j)\frac{k_s}{\gamma_j}\text{Im}\left(a_k^*\, e^{-i\theta_j}\right). \tag{20}$$

Comparing this relation with Eq.(1.a) shows that the power balance, Eq.(5) is exactly satisfied if in the equations for the longitudinal motion, the complex radiation field amplitude at a given particle j is approximated by the grid value a_k, with the index k related to j by $r_{k-1/2} \leq \sqrt{x_j^2 + y_j^2} < r_{k+1/2}$. This particle to grid interpolation is very similar to the so called NGP ("nearest grid point") scheme of the particle-in-cell simulation used in plasma physics [13].

3.3 Integration along the longitudinal direction

The radial dicretization of the wave equation, as described in the previous section yields a system of $2N_r$ real ordinary differential equations for the grid values of the radiation field; together with the equations for the particle phase space variables obtained in Sec.2.1, they form a system of $6N + 2N_r$ first order ODEs. One obvious way to solve this system of ODEs is to use existing ODE integrators found in most of the available numerical libraries. However, these general purpose routines are very expensive in terms of the CPU time as well as the computer central memory. For instance, the routine DGEAR in the IMSL library [15] requires a working array of (at least) 17 times the number of ODEs long! On the other hand, we should keep in mind that the field equation to be integrated, Eq.(16), is indeed only approximate, due to the radial discretization. This leads us to implement a simpler procedure of integration.

Let consider the interval on the z-axis defined by the end points z_{n-1}, $z_n = z_{n-1} + \Delta z$ and the central point $z_{n-1/2} = (z_{n-1} + z_n)/2$. The particle phase space variables $\{\gamma, \psi, p_x, x, p_y, y\}$ are assumed to be known at z_{n-1} and the radiation field discretized values a_k, at $z_{n-1/2}$. The marching algorithm can then be summarized as follows:

(a) Advance the particle variables from z_{n-1} to z_n, using a special low storage fourth order Runge-Kutta algorithm described in [16];

(b) Construct the source term s_k^n [second term in the right hand side of Eq.(16)];

(c) Solve, using the Gauss elimination, the following tridiagonal system of equations

$$\left[\mathbf{I} - i\frac{\Delta z}{4k_s}\mathbf{M}\right]\mathbf{a}^{n+1/2} = \left[\mathbf{I} + i\frac{\Delta z}{4k_s}\mathbf{M}\right]\mathbf{a}^{n-1/2} + \mathbf{s}^n\Delta z, \tag{21}$$

that results from Eq.(16) by replacing $d\mathbf{a}/dz$ and $\mathbf{a}$ at $z = z_n$, respectively with

$$\frac{\mathbf{a}^{n+1/2} - \mathbf{a}^{n-1/2}}{\Delta z}, \quad \text{and} \quad \frac{\mathbf{a}^{n+1/2} + \mathbf{a}^{n-1/2}}{2}. \tag{22}$$

In Eq.(21), the tridiagonal matrix $\mathbf{M}$ is defined in Eq.(17) and $\mathbf{I}$ designates the identity matrix.

Note that in the scheme described above, the wave equation source term $\mathbf{s}$ is centered on the interval $[z_{n-1/2}, z_{n+1/2}]$ while advancing $\mathbf{a}$ and similarly for the force term (proportional to $\mathbf{a}$) on the interval $[z_{n-1}, z_n]$, while advancing the particle phase space variables.

4. Code benchmarking

In order to benchmark the TDA code, we have performed (a) a comparison with the linear theory, and (b) a set of runs to analyze the convergence properties of the radial discretization used in the code. The free-electron-laser parameters used in these calculations are shown in Table 1.

In the linear theory, one-dimensional motion (no betatron oscillation) is assumed. The diffraction of the radiation field is, however, taken into account. Linearizing the single particle longitudinal equations of motion, Eqs.(1), and the paraxial wave equation, Eq.(4), and assuming a magnetostatic wiggler ($\omega_w = 0$) lead to the first order equations in a_s [17]:

$$\frac{\partial K_1}{\partial z} = \frac{k_w k_s f_B a_w}{\gamma_0} a_s e^{i(\phi_s + \mu_0 z)}, \tag{23.a}$$

$$\frac{\partial K_2}{\partial z} = K_1 - \frac{i k_s f_B a_w}{\gamma_0^2} a_s e^{i(\phi_s + \mu_0 z)}, \tag{23.b}$$

$$\left[\frac{\partial}{\partial z} + \frac{1}{2ik_s}\nabla_\perp^2\right] a_s e^{i\phi_s} = i\frac{eZ_0}{mc^2}\frac{f_B a_w}{2k_s}\frac{I}{\pi R_b^2} u(r) e^{-i\mu_0 z} K_2, \tag{23.c}$$

where the complex "macroscopic" variables $K_1(r,z)$ and $K_2(r,z)$ are respectively the velocity bunching amplitude and the density bunching amplitude defined by:

$$K_1 = ik_w \left\langle e^{-i\theta_0}(w_1 + w_1^*)\right\rangle, \quad K_2 = \left\langle e^{-i\theta_0} w_1\right\rangle, \tag{24}$$

Electron beam	
Energy γ	100.5
Energy spread $\Delta\gamma$	0.3
Radius R_b (mm)	0.26
Normalized emittance ϵ_n (mm mrad)	10
Wiggler field (magnetostatic)	
Period λ_w (cm)	3
On axis a_w	1
Bessel coefficient f_B	1
Length L (m)	5
Radiation field	
Wavelength λ_s (μm)	3
Rayleigh length Z_R (cm)	3
Focus Z_w (cm)	-20

Table 1. FEL parameters used for benchmarking TDA

with the angle brackets denoting the average over the particle initial phases (assuming a cold electron beam) and w_1 being the first order quantity in the expansion:

$$w \equiv e^{-i\theta}\gamma/\gamma_0 = e^{-i(\theta_0+\mu_0 z)}\left[1 + w_1 + \cdots\right]. \tag{25}$$

In Eqs.(23)–(25), γ_0, θ_0 and μ_0 denote the initial values for the electron Lorentz factor, phase and detuning parameter $\mu = k_w - (1+a_w^2)k_s/(2\gamma^2)$. In the source term of the wave equation, the electron beam has a prescribed radial density profile $u(r)$.

The system of equations (23) was solved in a separate code, using the same discretization in the radial direction for the wave equation as described in Sec.3.2. Notice that here, we have only 2 equations, instead of $6N$ in the nonlinear case, for describing the electron dynamics.

The comparison between the linear results and the nonlinear results are shown in

Fig. 1 for the radiation power and Fig. 2 for the radiation beam size. In the nonlinear calculations, 1024 simulation particles were used. In both calculations, there are 64 non-equidistant radial mesh points and 100 constant steps in the longitudinal direction ($\Delta z = 5\,\mathrm{cm}$). In the small-signal regime ($z < 2\,\mathrm{m}$), it is seen that the nonlinear results for the power gain as well as for the radiation beam size, agree well with the linear results. The larger gain obtained in the latter (23.5 dB/m compared to 23 dB/m) as well as the stronger radiation focusing effect are both consistent with the fact that both the energy spread and the finite emittance are omitted in the linear calculations.

In Figs. 3–5, we have varied the number of radial mesh intervals, N_r, keeping the particle number fixed at $N = 1024$ and the step size $\Delta z = 5\,\mathrm{cm}$. It can be seen that with $N_r = 64$, good convergence is already achieved for the radiation power $P_{\mathrm{rad}}(z)$ (Fig. 3), the radiation beam size $w(z)$ (Fig. 4) as well as the error in the power balance (plotted in Fig. 4 in % of the radiation power). The fact that the total power is well conserved, even in the $N_r = 32$ run, is a consequence of the chosen conservative scheme for the radial discretization (see Sec.3.2). The case with $N_r = 64$ was run again with 4096 particles, giving a difference of 0.2 % for P_{rad} and 0.8 % for w.

In Fig. 6, the values of the radiation power and the error in power conservation at the exit of the interaction region are plotted versus the square of the integration step size. It can be seen that for $\Delta z^2 < 50$ (more than 75 integration steps), the results show an almost quadratic convergence in Δz.

The CPU times (on a Cray-XMP,using the CFT compiler) for the three runs shown in Figs. 3–5 are 3.85, 4.18, 4.24 seconds respectively and thus are not very sensitive to N_r since the number of particle equations $6N$ is much larger than the number of discretized equations for the wave evolution. We have also checked that the CPU time used by TDA increases linearly with the number of particles N as well as the number of integration steps.

5. Conclusion

A particle simulation code, modeling the 3-D electron dynamics in an axisymmetric radiation field of an FEL has been developed and tested. A finite difference conservative scheme was employed to discretize the paraxial wave equation in the radial direction and proved to describe accurately the optical guiding effect in the high-gain FEL. In the longitudinal direction, a centered (in z) scheme was used to solve the wave equation, while a low storage fourth order Runge-Kutta integration was chosen to advance the particles. In order to model the electron distribution function at the entrance of the wiggler with a relatively small number of simulation particles ($\sim$ 1000–4000), "quiet start" techniques of particle loading have been used. Although effects such as electrostatic perturbations or non-circular electron beam effects are not considered, the physics contained in the TDA code is enough to give realistic gain performance for an FEL operating in the Compton regime. Since the present version of the TDA code is very fast, it can be served as an useful numerical tool for the development of more complex simulation codes for the FEL.

References

[1] P. Sprangle and C. M. Tang, *Appl. Phys. Lett.*, **39** (1981) 677.

[2] W. M. Kroll, P. L. Morton, and M. W. Rosenbluth, *IEEE J. Quantum Electron.*, **17** (1981) 1436.

[3] W. B. Colson, *IEEE J. Quantum Electron.*, **17** (1981) 1417.

[4] J. M. Slater and D. D. Lowenthal, *J. Appl. Phys.*, **52** (1981) 44.

[5] D. Prosnitz, A. Szoke, and V. K. Neil, *Phys. Rev. A*, **24** (1981) 1436.

[6] T. J. Orzechowski, B. Anderson, W. M. Fawley, D. Prosnitz, E. T. Scharlemann, S. Yarema, D. Hopkins, A. C. Paul, A. M. Sessler, and J. S. Wurtele, *Phys. Rev. Lett.*, **54** (1985) 889.

[7] J. Fajans, J. S. Wurtele, G. Bekefi, D. S. Knowles, and K. Xu, *Phys. Rev. Lett.*, **57** (1986) 579.

[8] A. Battacharjee, S. Y. Cai, S. P. Chan, J. W. Dodd, and T. C. Marshall, to be published in Proceedings of the Ninth International FEL Conference, Williamsburg, VA (1987).

[9] J. E. LaSala, D. A. G. Deacon, and E. T. Scharlemann, *Nucl. Instr. Methods Phys. Res. A*, **250** (1986) 19.

[10] T. M. Tran, B. G. Danly, and J. S. Wurtele, *IEEE J. Quantum Electron.*, **QE-23** (1987) 1578.

[11]] A. E. Siegman, *Lasers.* University Science Books, Mill Valley CA (1986).

[12] J. M. Hammersley and D. C. Handscomb, *Monte Carlo Methods*, Methuen, London, (1964).

[13] C. K. Birdsall and A. B. Langdon, *Plasma Physics via Computer Simulations*, McGraw-Hill, New-York (1985).

[14] E. T. Scharlemann, *J. Appl. Phys.*, **58** (1985) 2154.

[15] IMSL Library, *User's Manual, ed. 9.2*, Houston, TX (1984)

[16] E. K. Blum, *Math. Comp.*, **16** (1962) 176.

[17] G. T. Moore, *Nucl. Instr. Methods Phys. Res. A*, **239** (1985) 19.

Figure Captions

Fig. 1 Comparison between the linear theory and the simulation using 1024 particles for the radiation power evolution.

Fig. 2 Comparison between the linear theory and the simulation using 1024 particles for the radiation beam size evolution.

Fig. 3 Radiation power as a function of the longitudinal coordinate z for different values of the radial mesh intervals N_r.

Fig. 4 Error in the total power conservation, plotted in % of the *radiation power* as a function of the longitudinal coordinate z for different values of the radial mesh intervals N_r.

Fig. 5 Radiation beam size as a function of the longitudinal coordinate z for different values of the radial mesh intervals N_r.

Fig. 6 Radiation power and error in power conservation at the exit of the wiggler, plotted versus the square of the integration step size, showing a quadratic convergence in Δz.

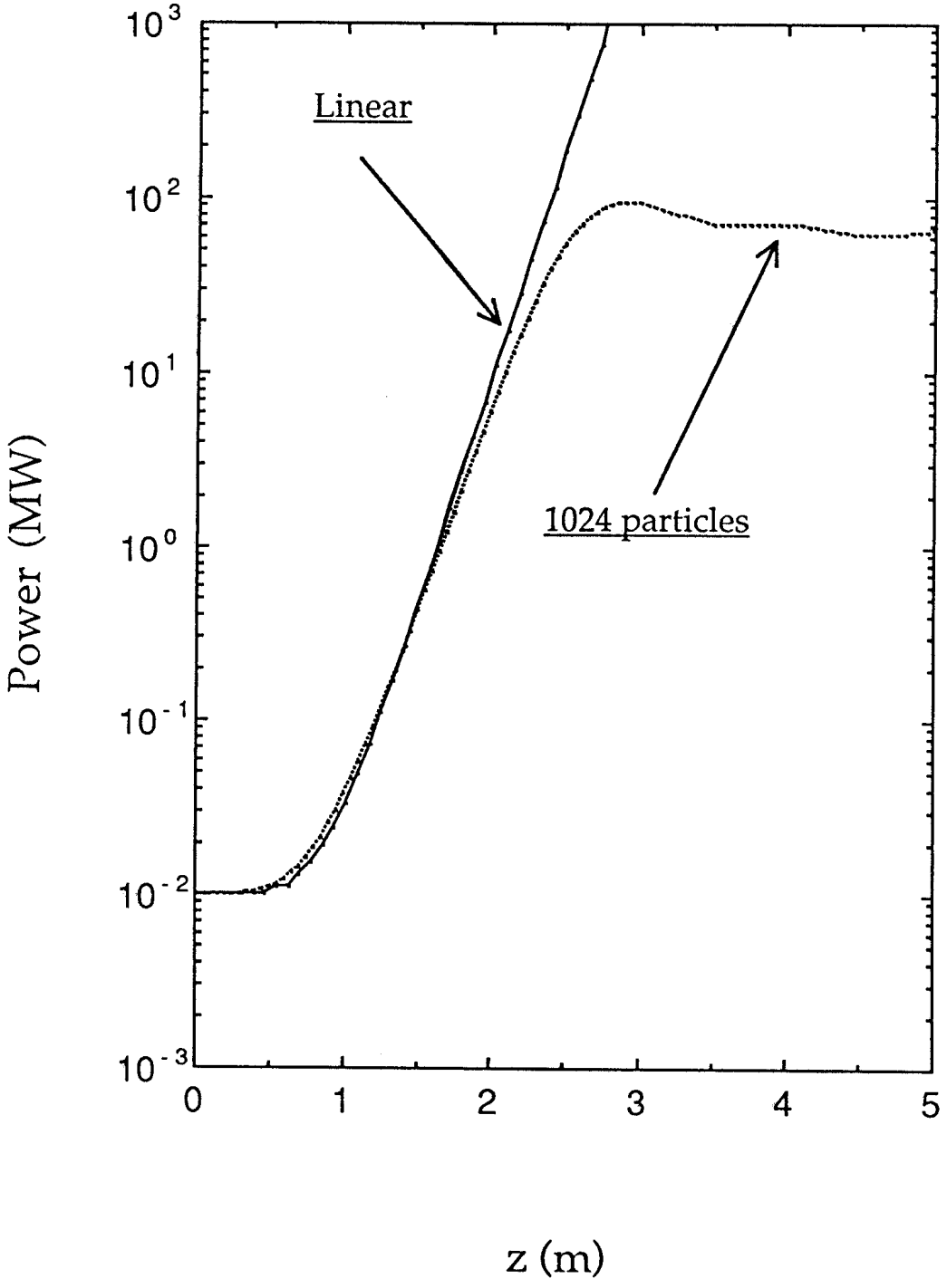
Power (MW)
10^3
10^2
10^1
10^0
10^{-1}
10^{-2}
10^{-3}
Linear
1024 particles
0
1
2
3
4
5
z (m)

Figure 1

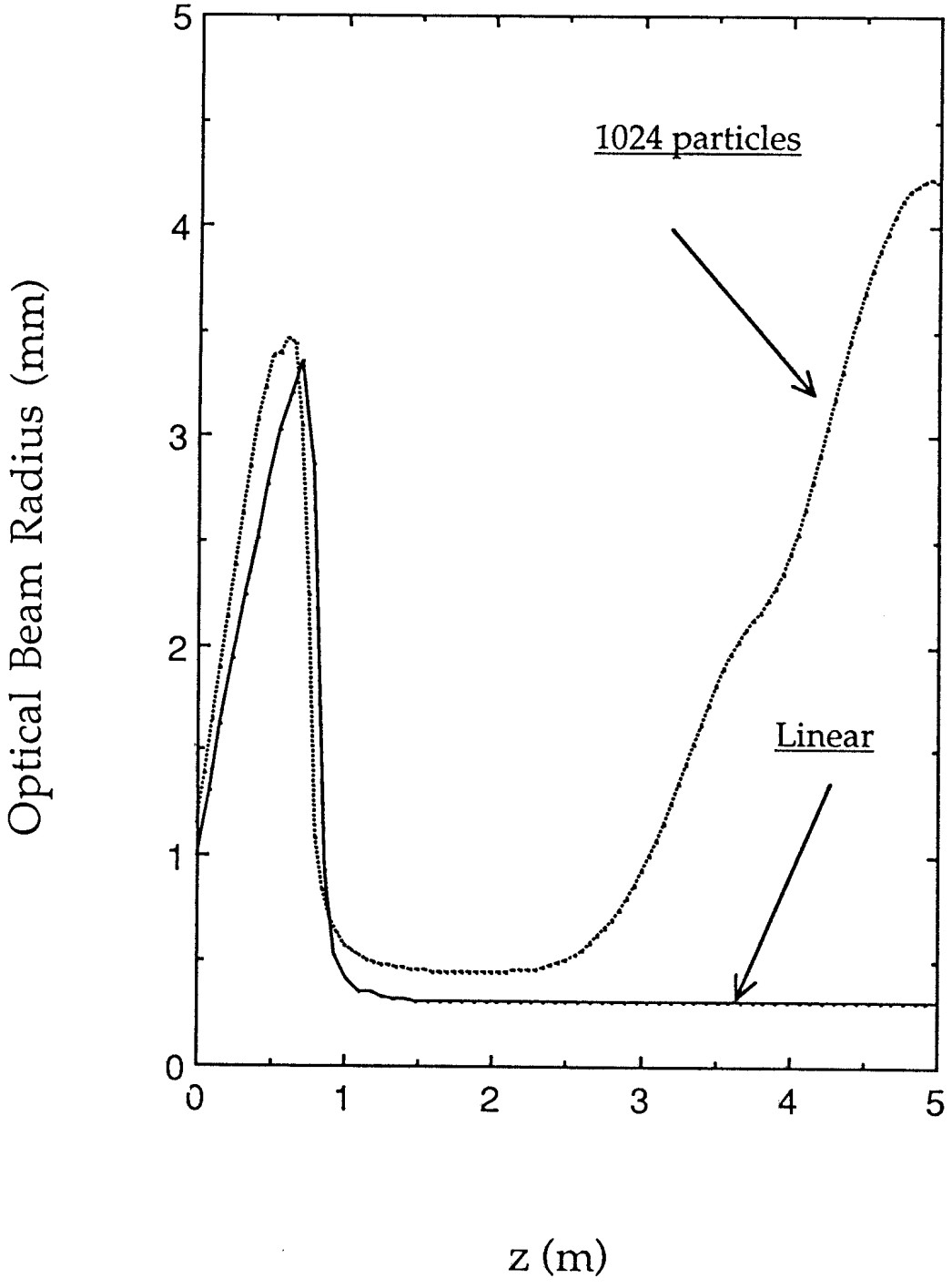

Figure 2

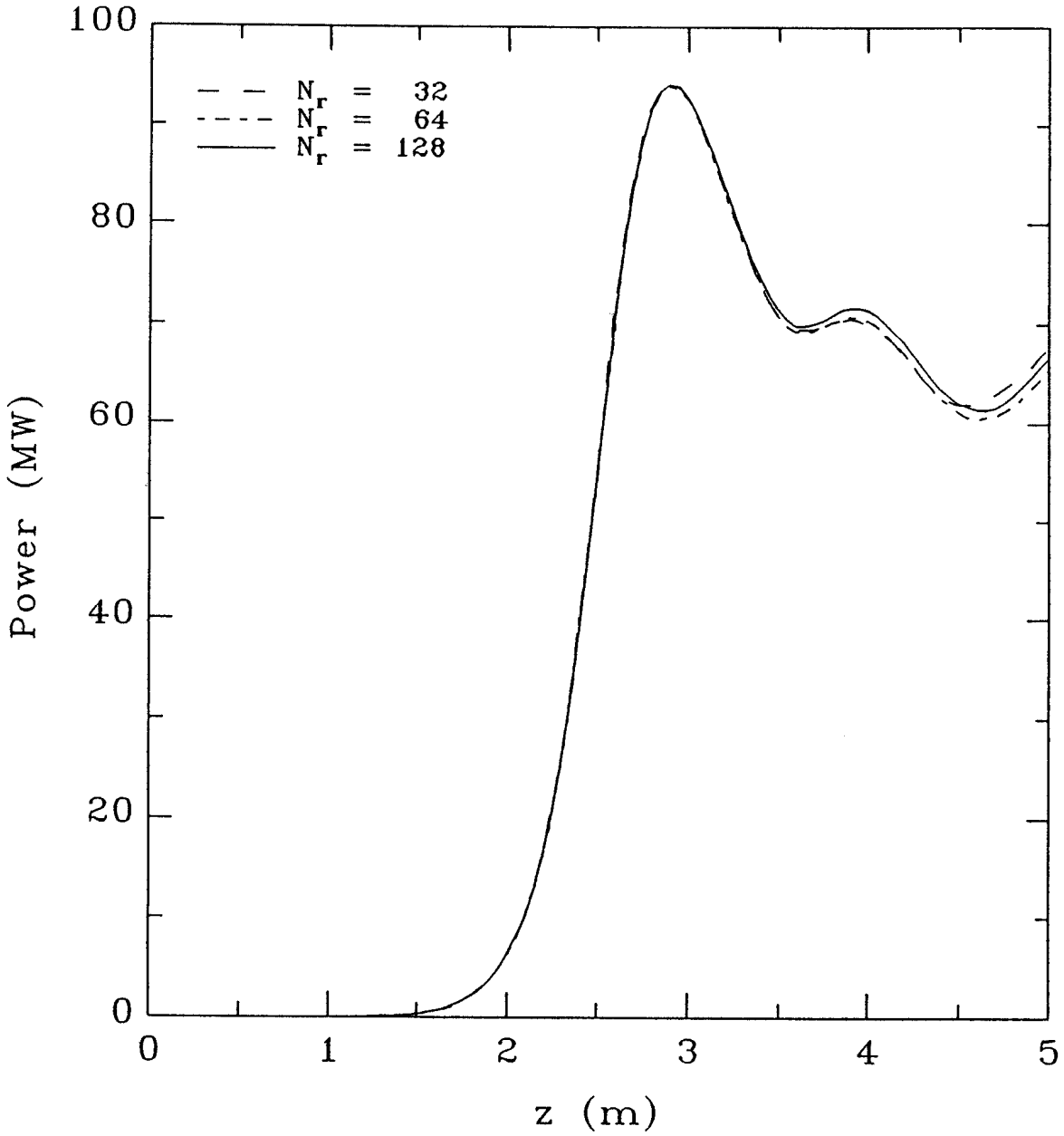

Figure 3

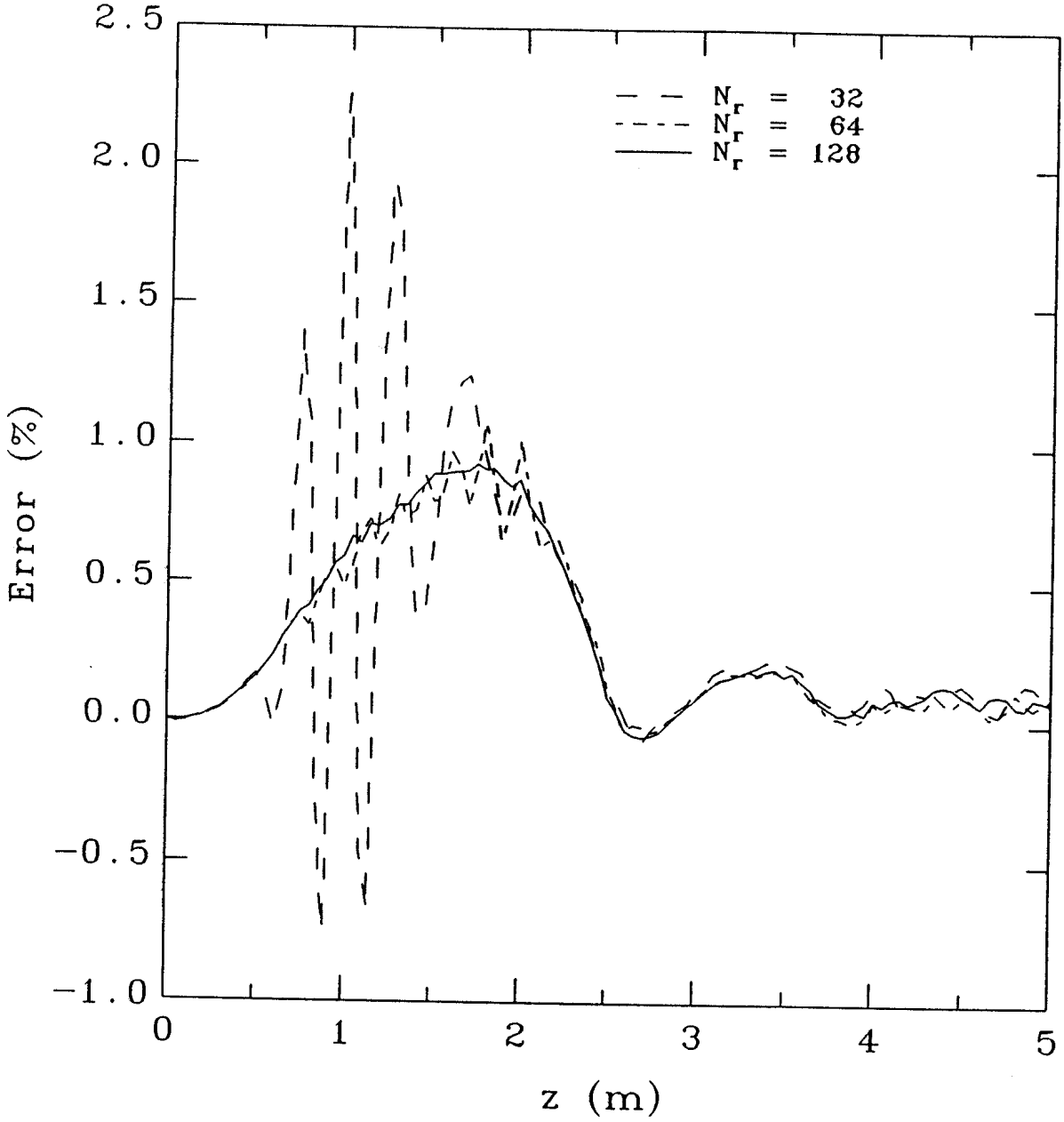

Figure 4

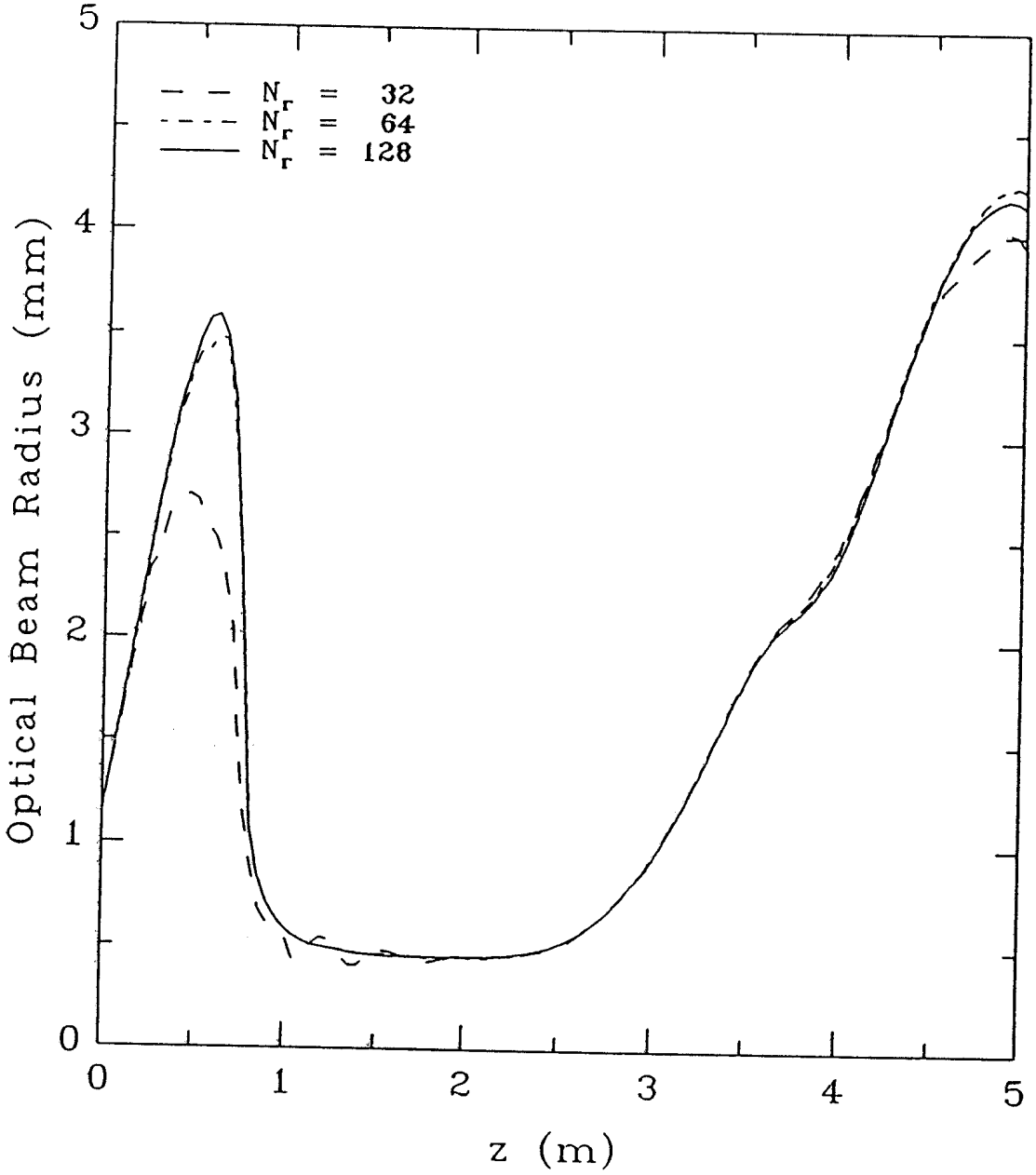

Figure 5

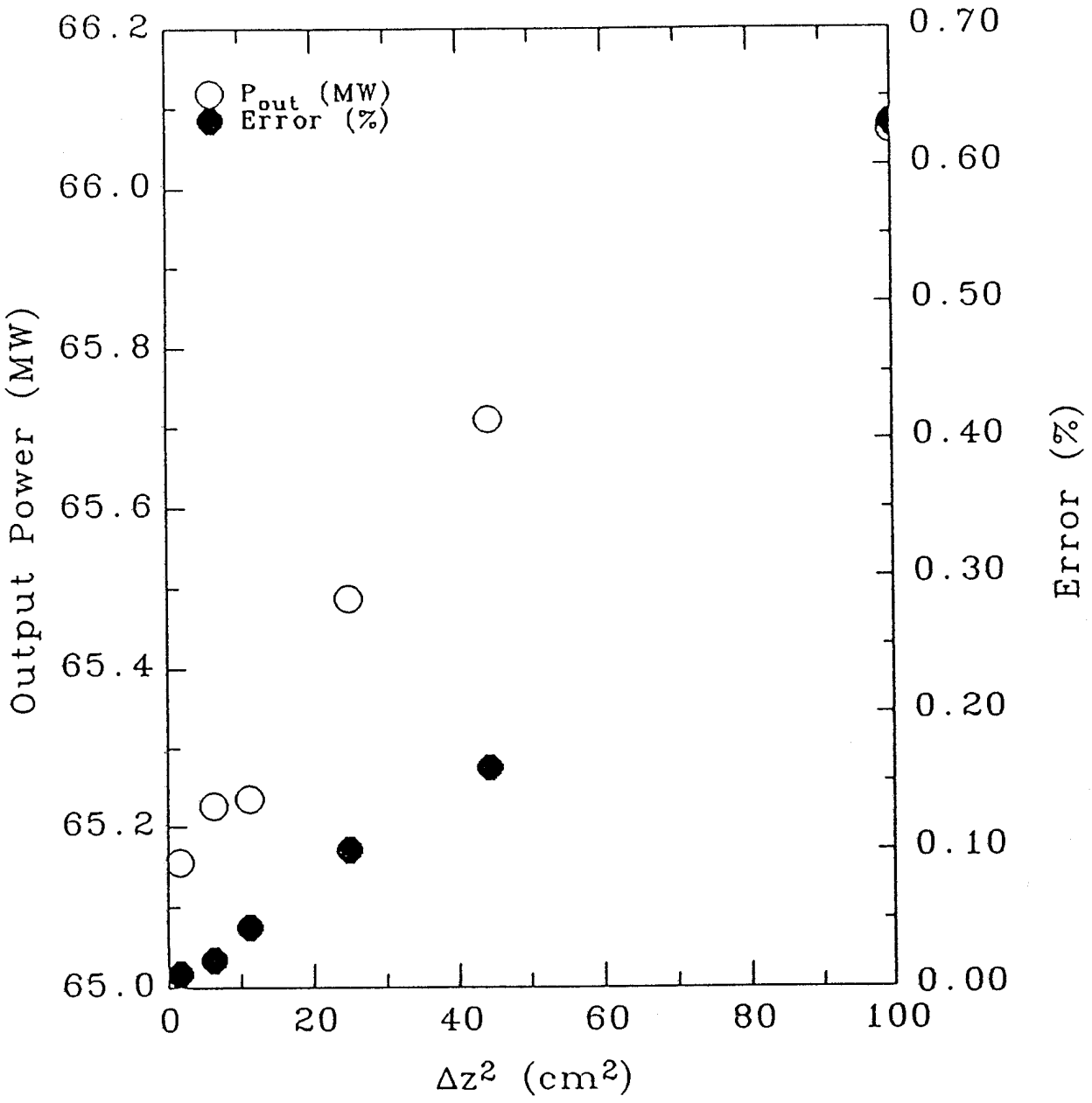
66.2
66.0
65.8
65.6
65.4
65.2
65.0
Output Power (MW)
0.70
0.60
0.50
0.40
0.30
0.20
0.10
0.00
Error (%)
P out (MW)
Error (%)
0
20
40
60
80
100
Δz² (cm²)

Figure 6